Synthesis of Mesoporous Silica Nanofibers with Controlled Pore Architectures

Jianfang Wang,[†,#] Chia-Kuang Tsung,[†] Wenbin Hong,[†,#] Yiying Wu,[†]
Jing Tang,[‡] and Galen D. Stucky*,[†,‡]

*Mitsubishi Chemical Center for Advanced Materials (MC-CAM),
Department of Chemistry and Biochemistry, and Materials Department,
University of California, Santa Barbara, California 93106*

Received June 17, 2004

A one-phase route has been developed for the synthesis, under strongly acidic conditions with cationic surfactants, of mesoporous silica nanofibers with controlled internal pore architectures. The diameters of the fibers range from 50 to 250 nm, and the lengths are up to millimeters. The nanofibers can have either a longitudinal pore architecture, in which the pore channels are aligned parallel to the fiber axis, or a circular pore architecture, in which the pore channels are wound circularly around the fiber axis. The pore channels in both types of nanofibers are hexagonally packed. The cross sections of the nanofibers with longitudinal pore architectures are hexagonal and those of the nanofibers with circular pore architectures are circular. Systematic experiments were carried out in which the fraction of the nanofibers with circular pore architectures among the overall nanofibers was determined as a function of the growth temperature for hexadecyltrimethylammonium chloride (C_{16}TMAC), hexadecyltrimethylammonium bromide (C_{16}TMAB), hexadecylpyridinium chloride (C_{16}PC), and hexadecylpyridinium bromide (C_{16}PB) surfactants. Generally, lower temperatures produce nanofibers with longitudinal pore architectures and higher temperatures produce nanofibers with circular pore architectures. The transition temperatures for C_{16}TMAC and C_{16}TMAB surfactants are around 75 °C and those for C_{16}PC and C_{16}PB surfactants are around 55 °C. In addition, the one-phase synthesis was carried out with cationic surfactants of different tail lengths, including dodecyltrimethylammonium bromide (C_{12}TMAB), tetradecyltrimethylammonium bromide (C_{14}TMAB), and octadecyltrimethylammonium bromide (C_{18}TMAB). No nanofibers are obtained from the synthesis with C_{12}TMAB or C_{14}TMAB surfactants, while greater than 95 wt % of the products from the synthesis with C_{18}TMAB surfactant are nanofibers with longitudinal pore architectures in the temperature range of 40−90 °C. Furthermore, rhodamine 6G (Rh6G) dye molecules were incorporated during growth to make mesostructured nanofibers that are millimeters long and fluoresce uniformly along the entire length of the individual fiber.

Introduction

The cooperative assembly between surfactant molecules and inorganic components provides a versatile approach to the creation of functional materials with potential applications in catalysis, separation, optoelectronics, biomaterials, and guest/host chemistry.[1−5] Since the discovery of mesoporous silica based on amphiphilic surfactant templates,[6,7] the use of surfactants to prepare mesoporous materials has been explored over a wide range of conditions. Such conditions have relied on various interactions, including electrostatic, hydrogen bonding, covalent bonding, and van der Waals forces, that have been balanced to achieve cooperative assembly and thereby direct the formation of mesostructures. Recently, many efforts have focused on developing mesoporous materials with hierarchical structures and well-defined shapes. Mesoporous spheres,[8−12] curve-shaped particles,[13−15] tubes,[16−18] fibers,[19,20] and thin films[21−26] have been prepared. Among these, mesopo-

---

[*] To whom correspondence should be addressed. E-mail: stucky@chem.ucsb.edu.

[†] Department of Chemistry and Biochemistry.

[#] MC−CAM.

[‡] Materials Department.

(1) De Vos, D. E.; Dams, M.; Sels, B. F.; Jacobs, P. A. *Chem. Rev.* **2002**, *102*, 3615.
(2) Scott, B. J.; Wirnsberger, G.; Stucky, G. D. *Chem. Mater.* **2001**, *13*, 3140.
(3) He, X.; Antonelli, D. *Angew. Chem., Int. Ed.* **2001**, *41*, 214.
(4) Ying, J. Y.; Mehnert, C. P.; Wong, M. S. *Angew. Chem., Int. Ed. Engl.* **1999**, *38*, 56.
(5) Bartl, M. H.; Puls, S. P.; Tang, J.; Lichtenegger, H. C.; Stucky, G. D. *Angew. Chem., Int. Ed.* **2004**, *43*, 3037.
(6) Kresge, C. T.; Leonowicz, M. E.; Roth, W. J.; Vartuli, J. C.; Beck, J. S. *Nature* **1992**, *359*, 710.
(7) Beck, J. S.; Vartuli, J. C.; Roth, W. J.; Leonowicz, M. E.; Kresge, C. T.; Schmitt, K. D.; Chu, C. T.-W.; Olson, D. H.; Sheppard, E. W.; McCullen, S. B.; Higgins, J. B.; Schlenker, J. L. *J. Am. Chem. Soc.* **1992**, *114*, 10834.
(8) Nooney, R. I.; Thirunavukkarasu, D.; Chen, Y. M.; Josephs, R.; Ostafin, A. E. *Chem. Mater.* **2002**, *14*, 4721.
(9) Fowler, C. E.; Khushalani, D.; Lebeau, B.; Mann, S. *Adv. Mater.* **2001**, *13*, 649.
(10) Lu, Y. F.; Fan, H. Y.; Stump, A.; Ward, T. L.; Rieker, T.; Brinker, C. J. *Nature* **1999**, *398*, 223.
(11) Huo, Q. S.; Feng, J. L.; Schüth, F.; Stucky, G. D. *Chem. Mater.* **1997**, *9*, 14.
(12) Grun, M.; Lauer, I.; Unger, K. K. *Adv. Mater.* **1997**, *9*, 254.

10.1021/cm049028q CCC: $27.50

rous fibers consisting of highly ordered and uniformly sized mesopores are of particular interest for optical devices because organic/inorganic nanoscale phase separation defining the mesostructure itself can provide chemically different environments for active optical species and thus allow for their doping with higher concentrations and protective packing into uniform three-dimensional arrays.[2] For example, they can be used as high-surface-area optical waveguides.[20] When doped with laser dyes, they can be used as a new type of laser material.[27,28]

Previous methods for creating mesoporous silica fibers include spinning, templating, and spontaneous growth. Spinning is based on the sol−gel process induced by rapid solvent evaporation from the solutions containing silica species and surfactant molecules. An important aspect of this method is that the solution viscosity must be carefully controlled. The fibers obtained typically have lengths of 3−10 cm and diameters of 5−100 μm.[29−31] For templated growth, individual strands of spider silk have been used to grow mesoporous fibers of 1−2 μm in diameter along the strands by dip coating,[32] and anodized alumina membranes have been used to grow mesoporous fibers of ~250 nm in diameter within the alumina pores.[33] Mesoporous fibers can also be obtained via spontaneous growth in liquid solutions. The method most often used is the two-phase reaction, in which fibers grow at a static oil−water interface under acidic conditions.[20,34−37] The resulting fibers are 100 μm−5 cm long and have diameters of 1−40 μm.

The pore channels of the mesoporous silica fibers that spontaneously grow at oil−water interfaces are highly organized. It was originally suggested that the pore channels are oriented parallel to the fiber axis.[20,37] However, later investigations indicated that the pore channels of the fibers obtained from the two-phase reactions are wound circularly around the fiber axis.[38−41] These different observations, on one hand, imply that the internal pore architectures of these fibers might depend strongly on the growth conditions, including the acid concentration, the growth temperature, and the concentrations of silica species and surfactants. On the other hand, the observations of the two types of internal pore architectures present an opportunity to synthesize mesoporous silica fibers with controlled pore architectures by systematically varying growth conditions. Investigations of the dependence of internal pore architectures on growth conditions could help in understanding the fundamental mechanism governing the cooperative assembly between surfactant molecules and inorganic components into three-dimensional mesostructures. Insight gained from such cooperative assembly processes is critical to the exploitation of organic and inorganic components in the fabrication of novel hybrid materials and even in the fabrication of devices using “bottom-up” approaches.

The pore channels that are packed hexagonally in mesoporous fibers can be oriented differently relative to the fiber axis. It is difficult to differentiate pore orientations on the basis of the low-angle X-ray diffraction (XRD) measurements on bulk amounts of the fiber samples. The mesoporous fibers obtained from the two-phase reactions have diameters on the micrometer scale, which limits the use of transmission electron microscopy (TEM) to characterize the internal pore architectures of individual fibers. The synthesis of mesoporous fibers with diameters down to the nanometer scale enables the use of TEM to investigate the pore structures of individual fibers. Information gained from the structural characterization of individual fibers can further be used to guide the choice of reaction conditions to synthesize mesoporous materials with specific internal pore architectures. Control of internal pore architectures is critical for advanced applications of mesoporous materials in areas such as controlled drug delivery[42] and membrane-based chemical and biochemical separations.[43]

We have developed a one-phase route to the synthesis of mesoporous silica nanofibers with diameters ranging from 50 to 250 nm and lengths up to millimeters using cationic surfactants and tetraethyl orthosilicate (TEOS) as the silica precursor.[44] The nanofibers are grown in dilute solutions of surfactants and silica species under strongly acidic conditions. They are single crystalline with hexagonally organized pore channels and possess either a circular pore architecture with the pore chan-

---

(13) Yang, S. M.; Yang, H.; Coombs, N.; Sokolov, I.; Kresge, C. T.; Ozin, G. A. *Adv. Mater.* **1999**, *11*, 52.

(14) Yang, H.; Ozin, G. A.; Kresge, C. T. *Adv. Mater.* **1998**, *10*, 883.

(15) Yang, H.; Coombs, N.; Ozin, G. A. *Nature* **1997**, *386*, 692.

(16) Lin, H.-P.; Mou, C.-Y.; Liu, S.-B. *Adv. Mater.* **2000**, *12*, 103.

(17) Lin, H.-P.; Cheng, S.; Mou, C.-Y. *Chem. Mater.* **1998**, *10*, 581.

(18) Lin, H.-P.; Mou, C.-Y. *Science* **1996**, *273*, 765.

(19) Yang, P. D.; Zhao, D. Y.; Chmelka, B. F.; Stucky, G. D. *Chem. Mater.* **1998**, *10*, 2033.

(20) Huo, Q. S.; Zhao, D. Y.; Feng, J. L.; Weston, K.; Buratto, S. K.; Stucky, G. D.; Schacht, S.; Schüth, F. *Adv. Mater.* **1997**, *9*, 974.

(21) Ruggles, J. L.; Holt, S. A.; Reynolds, P. A.; White, J. W. *Langmuir* **2000**, *16*, 4613.

(22) Miyata, H.; Kuroda, K. *J. Am. Chem. Soc.* **1999**, *121*, 7618.

(23) Zhao, D. Y.; Yang, P. D.; Melosh, N.; Feng, J. L.; Chmelka, B. F.; Stucky, G. D. *Adv. Mater.* **1998**, *10*, 1380.

(24) Lu, Y. F.; Ganguli, R.; Drewien, C. A.; Anderson, M. T.; Brinker, C. J.; Gong, W. L.; Guo, Y. X.; Soyez, H.; Dunn, B.; Huang, M. H.; Zink, J. I. *Nature* **1997**, *389*, 364.

(25) Yang, H.; Coombs, N.; Sokolov, I.; Ozin, G. A. *Nature* **1996**, *381*, 589.

(26) Yang, H.; Kuperman, A.; Coombs, N.; Mamiche-Afara, S.; Ozin, G. A. *Nature* **1996**, *379*, 703.

(27) Loerke, J.; Marlow, F. *Adv. Mater.* **2002**, *14*, 1745.

(28) Marlow, F.; McGehee, M. D.; Zhao, D. Y.; Chmelka, B. F.; Stucky, G. D. *Adv. Mater.* **1999**, *11*, 632.

(29) Madhugiri, S.; Zhou, W. L.; Ferraris, J. P.; Balkus, K. J., Jr. *Microporous Mesoporous Mater.* **2003**, *63*, 75.

(30) Jung, K. T.; Chu, Y.-H.; Haam, S.; Shul, Y. G. *J. Non-Cryst. Solids* **2002**, *298*, 193.

(31) Bruinsma, P. J.; Kim, A. Y.; Liu, J.; Baskaran, S. *Chem. Mater.* **1997**, *9*, 2507.

(32) Huang, L. M.; Wang, H. T.; Hayashi, C. Y.; Tian, B. Z.; Zhao, D. Y.; Yan, Y. S. *J. Mater. Chem.* **2003**, *13*, 666.

(33) Yang, Z. L.; Niu, Z. W.; Cao, X. Y.; Yang, Z. Z.; Lu, Y. F.; Hu, Z. B.; Han, C. C. *Angew. Chem., Int. Ed.* **2003**, *42*, 4201.

(34) Kanno, H.; Oumii, Y.; Kodaira, T.; Teranishi, T.; Sano, T. *J. Ceram. Soc. Jpn.* **2003**, *111*, 502.

(35) Alsyouri, H. M.; Lin, Y. S. *Chem. Mater.* **2003**, *15*, 2033.

(36) Kleitz, F.; Marlow, F.; Stucky, G. D.; Schüth, F. *Chem. Mater.* **2001**, *13*, 3587.

(37) Schacht, S.; Huo, Q.; Voigt-Martin, I. G.; Stucky, G. D.; Schüth, F. *Science* **1996**, *273*, 768.

(38) Marlow, F.; Kleitz, F. *Microporous Mesoporous Mater.* **2001**, *44*−*45*, 671.

(39) Kleitz, F.; Wilczok, U.; Schüth, F.; Marlow, F. *Phys. Chem. Chem. Phys.* **2001**, *3*, 3486.

(40) Marlow, F.; Zhao, D. Y.; Stucky, G. D. *Microporous Mesoporous Mater.* **2000**, *39*, 37.

(41) Marlow, F.; Spliethoff, B.; Tesche, B.; Zhao, D. Y. *Adv. Mater.* **2000**, *12*, 961.

(42) Lai, C.-Y.; Trewyn, B. G.; Jeftinija, D. M.; Jeftinija, K.; Xu, S.; Jeftinija, S.; Lin, V. S.-Y. *J. Am. Chem. Soc.* **2003**, *125*, 4451.

(43) Jirage, K. B.; Hulteen, J. C.; Martin, C. R. *Science* **1997**, *278*, 655.

(44) Wang, J. F.; Zhang, J. P.; Asoo, B. Y.; Stucky, G. D. *J. Am. Chem. Soc.* **2003**, *125*, 13966.

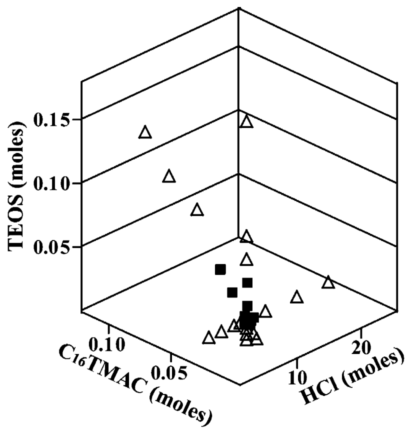

Figure 1. Optimization of the reaction composition for growing mesoporous silica nanofibers. Solid squares represent the reaction compositions for which both nanofibers and particles were obtained, and triangles represent the reaction compositions for which only particles were obtained. The mole numbers of HCl, C_{16}TMAC, and TEOS are with respect to 100 mole H_2O.

nels running circularly around the fiber axis or a longitudinal pore architecture with the pore channels oriented parallel to the fiber axis. The internal pore architectures of these nanofibers are highly dependent on the growth temperature and the surfactant that are used. In general, lower temperatures produce nanofibers with longitudinal pore architectures and higher temperatures produce nanofibers with circular pore architectures for C_{16}TMAC, C_{16}TMAB, C_{16}PC, and C_{16}PB surfactants. The transition temperature from the longitudinal to circular pore architecture is found to be dependent on the surfactant headgroup. In contrast, the internal pore architectures of the nanofibers synthesized with C_{18}TMAB surfactant are always longitudinal and are independent of the growth temperature.

Experimental Section

Synthesis. The one-phase route to the synthesis of mesoporous nanofibers was carried out in dilute solutions of cationic surfactants and silica species under strongly acidic conditions. The synthesis was started with mixing calculated amounts of cationic surfactants, distilled water, and concentrated HCl. The mixture was stirred until the surfactant molecules were dissolved completely. A calculated amount of TEOS was then added. The resulting solution was stirred at room temperature for 10 min and then transferred to a 60 mL glass vessel. The vessel was closed and kept in an isothermal oven at a certain temperature for ~2 days. Before the reaction mixture was moved into the isothermal oven, a small amount of aggregated particles appeared in the clear solution. After being kept in the oven for ~10 min, the reaction solution became turbid. The solution stayed turbid for ~40 min and then became clear again. During this period of time, fiberlike flocculates suspended in the solution started to form, and more aggregated particles were observed to precipitate at the bottom of the vessel. After growth, both the fiberlike flocculates and the particles were taken out separately with care. They were washed with distilled water three times and dried at 100 °C in air. To remove cationic surfactants, dried fiberlike flocculates and particles were calcined in a box furnace in air at 500 °C for 5 h, with a ramp rate of 1 °C/min.

We systematically varied the reaction composition for growing mesoporous silica nanofibers. Figure 1 summarizes the results from the synthesis with C_{16}TMAC surfactant at ~80 °C. It was found that the optimal composition, the one that can give the largest yield of fiberlike flocculates, is around 100 H_2O/7.0 HCl/0.02 C_{16}TMAC/0.03 TEOS (in molar ratio). This optimal composition was further used for the surfactants of hydrophobic hexadecyl tails to investigate the temperature dependence of the internal pore architectures of mesoporous nanofibers. The compositions for the syntheses using C_{12}TMAB, C_{14}TMAB, and C_{18}TMAB surfactants were 100 H_2O/7.0 HCl/0.30 C_{12}TMAB/0.45 TEOS, 100 H_2O/7.0 HCl/0.04 C_{14}TMAB/0.06 TEOS, and 100 H_2O/7.0 HCl/0.006 C_{18}TMAB/0.009 TEOS, respectively, because the critical micelle concentrations of C_{12}TMAB and C_{14}TMAB are larger than that of C_{16}TMAB and the critical micelle concentration of C_{18}TMAB is smaller than that of C_{16}TMAB.

We also obtained fluorescent nanofibers by adding a calculated amount of Rh6G to surfactant solutions during synthesis. The reaction composition for growing fluorescent nanofibers was 100 H_2O/7.0 HCl/0.02 C_{16}TMAC/0.03 TEOS/0.0002–0.0005 Rh6G.

Characterization. Low-angle XRD patterns were obtained on a Scintag PADX diffractometer using Cu Kα radiation. Scanning electron microscopy (SEM) studies were performed on a JEOL 6340F microscope operating at 2–5 keV. TEM studies were carried out on a JEOL 2010 microscope operating at 200 keV. To be able to observe the cross sections of nanofibers, microtoming was used to cut thin slices of ~70 nm thickness off a solidified thermocurable resin embedded with nanofiber samples. Nitrogen sorption isotherms were measured using a Micromeritics TriStar 3000 system at 77 K. The sorption data were analyzed using the Barrett–Joyner–Halenda (BJH) model with the Halsey equation for multilayer thickness. The pore size distribution was obtained from the analysis of the adsorption branch. The total pore volume was taken at the single point at a relative pressure of 0.99. A Netzsch thermoanalyzer STA 409 was used for simultaneous thermogravimetric analysis (TGA) and differential thermal analysis (DTA) with a heating rate of 5 °C/min in air. A Nikon optical microscope was used to obtain fluorescence images and spectra of mesostructured nanofibers doped with Rh6G (more characterization details are given in the Supporting Information).

Results and Discussion

Synthesis Products. After growth, the fiberlike flocculates are suspended in the growth solution, which naturally separates them from the aggregated particles precipitated at the bottom. The yield of the fiberlike flocculates from each synthesis with the optimal reaction composition is 5–30 wt %. In general, syntheses at lower temperatures produce fewer fiberlike flocculates. SEM imaging indicates that the flocculates mainly consist of fibers of lengths ranging from tens of micrometers to millimeters (Figure 2a and 6a) and the precipitates are micrometer-sized curve-shaped particles, including toroidal, disklike, spiral, and spheroidal shapes (see Figure S1 in the Supporting Information). Particles with similar morphologies have been obtained previously under different growth conditions.[13–15] A small number of curve-shaped particles are also present together with the fibers, probably because they are aggregated with or supported by the entangled fibers in the solutions during growth.

The optimal reaction composition for our one-phase route to the synthesis of mesoporous nanofibers is around 100 H_2O/7.0 HCl/0.02 surfactant/0.03 TEOS for the surfactants with hydrophobic hexadecyl tails (Figure 1). For comparison, previous two-phase syntheses of mesoporous fibers with micrometer-sized diameters have been conducted at room temperature with a typical reaction composition of 100 H_2O/2.9 HCl/0.025 C_{16}TMAB/0.054 TEOS.[20,37] In addition, the reaction com-

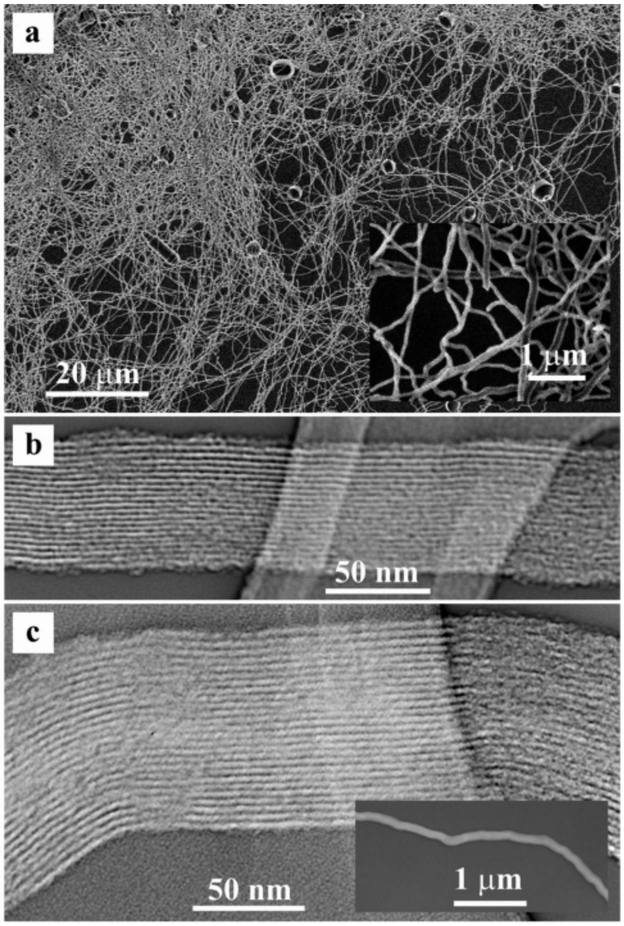

Figure 2. (a) SEM image of as-synthesized silica nanofibers. (b) and (c) TEM images of as-synthesized nanofibers. The inset to (a) is a zoomed-in SEM image. The inset to (c) is a low-magnification TEM image of one nanofiber. The nanofibers were prepared with C_{16}TMAC surfactant at 50 °C.

position for the quiescent growth of mesoporous thin films at the air−water interface is 100 H_2O/7.0 HCl/0.11 C_{16}TMAC/0.07−0.13 TEOS,[25] the composition for the quiescent growth of curve-shaped particles is 100 H_2O/3.5−7.0 HCl/0.1 C_{16}TMAC/0.1 TEOS,[13−15] and the composition for the first synthesis of SBA-3 materials[45−48] is 100 H_2O/7.1 HCl/0.092 C_{16}TMAB/0.77 TEOS. Our one-phase synthesis of mesoporous silica nanofibers is carried out in much more dilute surfactant and silica solutions under strongly acidic conditions, with an acid concentration of ~3.9 M.

During the previous two-phase synthesis of mesoporous fibers, silica precursor molecules are dissolved in the oil phase and surfactant molecules are dissolved in the water phase. Silica precursor molecules first diffuse from the oil phase through the interface to the water phase, where they are hydrolyzed. The resulting silica monomers and oligomers then cooperatively assemble with surfactant molecules to form mesostructured products, the morphologies of which strongly depend on the silica supply and on the assembly process between the silica species and surfactant molecules in the water phase region close to the interface.[20,37] In our one-phase synthesis, silica precursor molecules are quickly added into the aqueous surfactant solution and hydrolyzed within several minutes under strongly acidic conditions. The resulting silica species are homogeneously dissolved in the aqueous solution. The morphologies of the resulting products are solely determined by the cooperative assembly process between the silica species and surfactant molecules in the growth solution. This simple route offers the opportunity for further control of the shapes and pore orientations of mesostructured products by systematically varying the synthetic parameters.

Nanofibers with Longitudinal Pore Architectures. Figure 2a shows a typical SEM image of the mesoporous fibers grown with C_{16}TMAC surfactant at ~50 °C. Most of the fibers have diameters smaller than 100 nm. Each fiber has a uniform diameter and there are kinks along the fiber axis (Figure 2, parts a and c, insets). High-magnification TEM images show that the pore channels of these fibers are aligned parallel to the fiber axis (Figure 2, parts b and c); that is, they have a longitudinal pore architecture. At the positions of kinks, the parallel pore channels are continuous and all bend toward the same direction (Figure 2c). During TEM imaging, it is also observed that well-separated pore channels often disappear along the fiber axis (Figure 2b). The disappearance of pore channels under TEM imaging suggests that the nanofibers are slightly twisted.

The pore channels of the nanofibers with longitudinal pore architectures are highly organized. Figure 3b shows a line profile extracted from the digitized TEM image of a 208 nm diameter fiber, as shown in Figure 3a. The spacings between neighboring parallel pore channels determined from this line profile are shown in Figure 3c. They fluctuate around an average of 4.07 nm, indicating that the pore channels are equally spaced.

The possession of kinks is a unique feature of the nanofibers with longitudinal pore architectures. We have imaged more than 500 nanofibers of this type using TEM and found that the nanofibers with kinks along the fiber axis always exhibit longitudinal pore architectures. Each nanofiber possesses a large number of kinks. These kinks have various curvatures and bending directions. The spacing between neighboring kinks along a single fiber ranges from 150 to 500 nm. In addition, the kinks are stable during TEM imaging. These observations indicate that the kinks probably form during the nanofiber growth. If a nanofiber is perturbed during its growth and the pore channels on one side grow faster than those on the other side, the nanofiber will bend toward the side of slower growth. On the other hand, if a nanofiber were bent after its growth, there would be tensile stress on the outer side and compressive stress on the inner side of the nanofiber at the bending location. The presence of a large number of kinks would consume a large amount of elastic energy.

The TEM images shown in Figures 2 and 3 were taken with the viewing direction perpendicular to the fiber axis. A perspective of how the parallel pore channels are packed together was obtained by imaging nanofibers with the viewing direction parallel to the

---

(45) Huo, Q. S.; Margolese, D. I.; Stucky, G. D. *Chem. Mater.* **1996**, *8*, 1147.

(46) Huo, Q. S.; Leon, R.; Petroff, P. M.; Stucky, G. D. *Science* **1995**, *268*, 1324.

(47) Huo, Q. S.; Margolese, D. I.; Ciesla, U.; Feng, P. Y.; Gier, T. E.; Sieger, P.; Leon, R.; Petroff, P. M.; Schüth, F.; Stucky, G. D. *Nature* **1994**, *368*, 317.

(48) Huo, Q. S.; Margolese, D. I.; Ciesla, U.; Demuth, D. G.; Feng, P. Y.; Gier, T. E.; Sieger, P.; Firouzi, A.; Chmelka, B. F.; Schüth, F.; Stucky, G. D. *Chem. Mater.* **1994**, *6*, 1176.

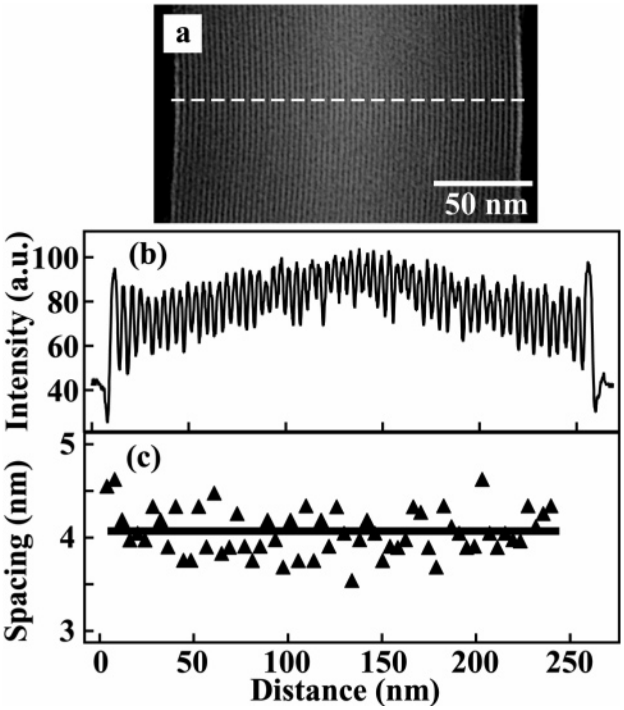

Figure 3. (a) TEM image of an as-synthesized fiber with the pore channels aligned parallel to the fiber axis. (b) An intensity profile extracted from the digitized TEM image along the dashed line shown in (a). (c) The spacings between neighboring parallel pore channels determined from (b). The solid line is the average spacing. The background in (b) is due to the nonuniform distribution of electron beam intensity. The fiber was prepared with C$_{16}$TMAC surfactant at 50 °C.

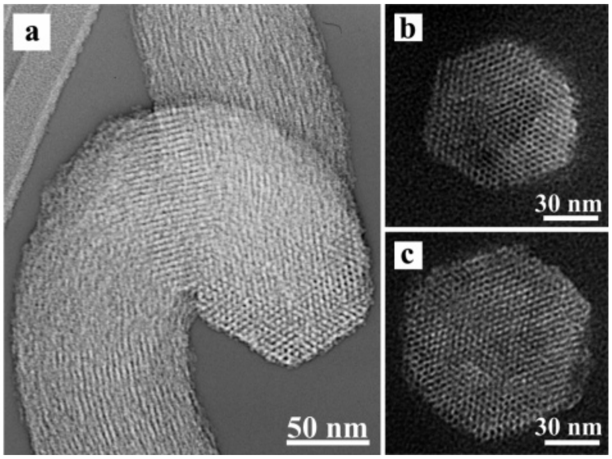

Figure 4. (a) TEM image of a fiber with a short section oriented perpendicular to the TEM grid plane. (b) and (c) TEM images taken on microtomed nanofiber samples. The nanofiber samples were synthesized with C$_{16}$TMAC surfactant at 50 °C and prepared for TEM imaging without calcination.

fiber axis (Figure 4). In our experiments, the nanofiber samples for TEM imaging were prepared by applying a few drops of the ethanol solution dispersed with nanofibers onto TEM grids. In this way, nanofibers always stay on the grids with their long axes parallel to the grid plane due to their extremely large aspect ratios. However, due to the presence of closely spaced kinks along the fiber axis, sometimes short sections of nanofibers between two neighboring kinks are seen to be oriented perpendicular to the grid plane, allowing for imaging the cross sections of nanofibers, as shown in Figure 4a. It is observed that the overall cross section of each nanofiber is hexagonal instead of circular and that the pore channels aligned parallel to the fiber axis are hexagonally packed together. To confirm these observations, we further embedded the nanofiber samples with longitudinal pore architectures into a resin and cut slices of $\sim$70 nm thickness by microtoming. It happens that some nanofibers can be cut perpendicular to their long axes. The TEM images (Figure 4, parts b and c) taken on microtomed fibers clearly reveal that the overall cross sections of the nanofibers with longitudinal pore architectures are hexagonal and that the pore channels in these nanofibers are hexagonally organized.

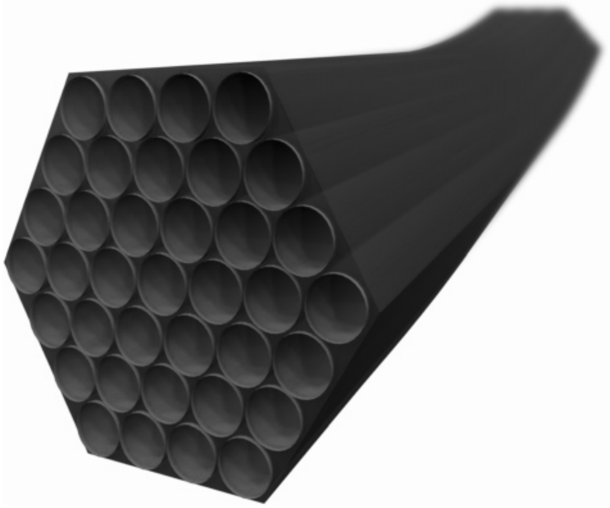

Figure 5. Three-dimensional model of a nanofiber with a longitudinal pore architecture.

Side-view TEM images in conjunction with cross-sectional TEM images show unambiguously that the nanofibers with longitudinal pore architectures consist of parallel pore channels hexagonally packed together. These pore channels are micrometers long and a few nanometers thick. They stay continuous at the positions of kinks. On the basis of these structural observations, a three-dimensional model can be built for the nanofibers with longitudinal pore architectures (Figure 5). When one nanofiber is oriented with one of the $\langle 010\rangle$ directions parallel to the viewing direction, the pore channels aligned parallel to the fiber axis are visible during TEM imaging, and the (100) interplanar spacing is measured to be 4.07 nm (Figure 3). For comparison, the lattice constant, a, determined from the cross-sectional TEM images and low-angle XRD patterns taken on as-synthesized nanofiber samples is 4.72 nm. The measured (100) interplanar spacing is approximately $\sqrt{3}/2$ of the lattice constant, which is in agreement with the two-dimensional hexagonal lattice. For a nanofiber with a cross-sectional area equal to that of a circle with a diameter of 85 nm, the typical size of the nanofibers with longitudinal pore architectures, the number of the pore channels packed in the nanofiber is estimated to be 300. It is remarkable that hundreds of pore channels up to hundreds of micrometers long can bind together in a highly ordered array to form a mesoporous nanofiber.

Nanofibers with Circular Pore Architectures. As discussed above, mesoporous nanofibers with longitudinal pore architectures can be synthesized at growth

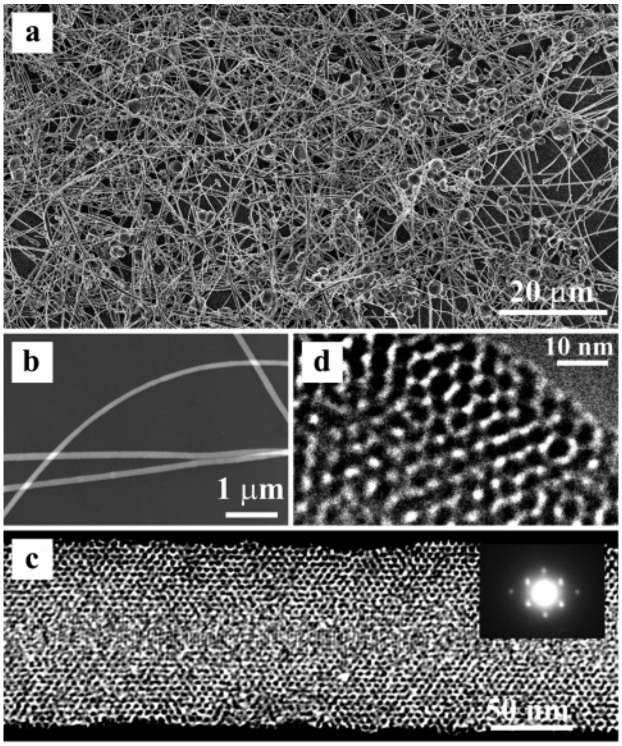

Figure 6. (a) SEM image of mesoporous silica nanofibers. (b) Low-magnification TEM image of the nanofibers. (c) High-magnification TEM image of one nanofiber. The inset is a selected-area electron diffraction pattern of the nanofiber. (d) High-resolution TEM image recorded at the edge of one nanofiber. The nanofibers were synthesized with C_{16}TMAC surfactant at 85 °C. The nanofiber samples for SEM and TEM observations were as synthesized without calcination.

temperatures around 50 °C. We tried growing mesoporous nanofibers at different temperatures to see if we can control the internal pore architecture. Figure 6a shows a typical SEM image of the fibers grown with the same synthetic procedure and reaction composition as those shown in Figure 2, but at ~85 °C. The samples mainly consist of fibers about 100 nm thick and hundreds of micrometers long. SEM imaging, together with TEM imaging at low magnifications (Figure 6b), indicates that a majority of the nanofibers have uniform diameters along their long axes and that they are smooth without the kinks as seen on the nanofibers grown at the lower temperature. TEM images at high magnifications show hexagonally packed pore channels at the edges of each nanofiber (Figure 6c). This hexagonal ordering of the pore channels is further confirmed by the selected-area electron diffraction patterns (Figure 6c, inset) and high-resolution TEM images taken on individual nanofibers (Figure 6d). Similar diffraction patterns have previously been obtained with a highly collimated X-ray source and an array detector on the two-phase-synthesized fibers, the pore channels of which are wound circularly around the fiber axis.[49]

Unlike the nanofibers with longitudinal pore architectures, the pore channels of which aligned parallel to the fiber axis often disappear because the nanofibers are twisted, the hexagonal array of the pore channels is observed over the entire length of individual nanofibers grown at the higher temperature. This indicates strongly that the organization of the pore channels in this type of nanofiber is circularly symmetric; that is, these nanofibers have circular pore architectures. To confirm the presence of such circular symmetry, TEM images were taken at the ends of the nanofibers. It is seen from the nanofibers with rough ends that the pore channels are aligned circularly around the fiber axis (Figure 7a). TEM images were also taken under a slightly defocused condition, where parallel fringes perpendicular to the fiber axis are visible in the central regions of individual nanofibers (Figure 7b), indicating that the pore channels in these nanofibers are oriented perpendicular to the fiber axis. The facts that hexagonally packed pore channels are clearly visible at both edges of individual nanofibers simultaneously and that they appear as parallel fringes perpendicular to the fiber axis under a slightly defocused condition suggest that these pore channels are either circular rings or helices with an extremely small pitch of one or only a few lattice constants. A large pitch displacement would require tilting of individual nanofibers to view exactly in the channel direction. TEM imaging was further performed on microtomed thin sections of the nanofibers to see the cross sections. Two representative images are shown in Figure 7, parts c and d, where the diameters of the two fibers are 110 and 105 nm, respectively. The pore channels are visible as concentric rings, and the overall cross sections of the nanofibers are circular. These circular pore channels converge into a single straight pore channel at the fiber center, which can be thought of as a natural singularity. The growth of the nanofibers with circular pore architectures might be governed by this straight pore channel at the fiber center. The

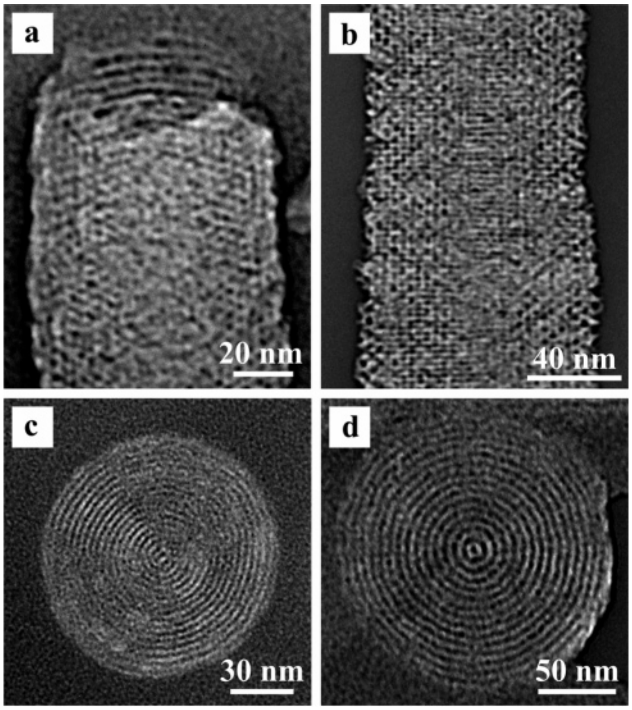

Figure 7. (a) TEM image of the end of one nanofiber. (b) TEM image of one nanofiber taken under a slightly defocused condition. (c) and (d) Cross-sectional TEM images taken on microtomed nanofiber samples. The nanofiber samples were synthesized with C_{16}TMAC surfactant at 85 °C and prepared for TEM imaging without calcination.

---

[49] Marlow, F.; Leike, I.; Weidenthaler, C.; Lehmann, C. W.; Wilczok, U. *Adv. Mater.* **2001**, *13*, 307.

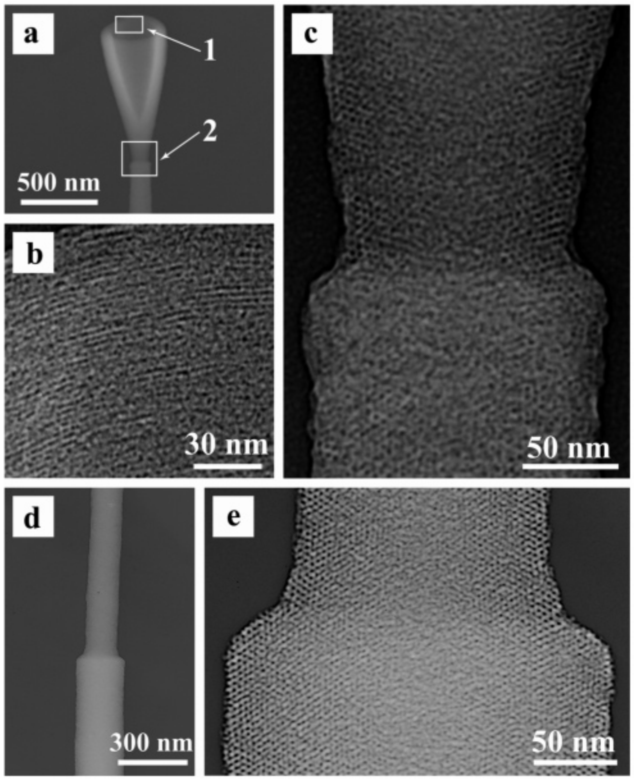

Figure 8. (a) TEM image of an antiumbrella structure at the end of one nanofiber. (b) and (c) are zoomed-in TEM images of the boxed areas labeled 1 and 2 in (a). (d) TEM image of a nanofiber junction. (e) Zoomed-in TEM image of the nanofiber junction shown in (d). The nanofibers were synthesized with C_{16}TMAC surfactant at 85 °C and prepared for TEM imaging without calcination.

concentric pore channels have also been observed before in the micrometer-sized fibers prepared with the two-phase reactions[38−41] and those made with anodized alumina pores as templates.[33]

As noted above, a variety of curve-shaped morphologies have been reported for mesoporous silica particles synthesized under different conditions.[13−15] Similarly, additional morphological shapes have also been observed here for the nanofibers with circular pore architectures, such as antiumbrellas, junctions, and artistic table legs. Their total yield is estimated from SEM imaging to be less than 5 wt % among all the nanofibers. Figure 8a shows a low-magnification TEM image of an antiumbrella structure grown at the end of one fiber, which acts as the umbrella stand. There is a junction between the stand and the umbrella central pole, from which the umbrella screen radiates. The stand has a diameter of 155 nm, and the central pole has a diameter of 118 nm. The screen is 59 nm thick, and it opens with a maximal outer diameter of 870 nm. The pore channels in the screen, the central pole, and the stand are all wound circularly around the central axis, as shown in Figure 8, parts b and c.

The junction shown in Figure 8, parts a and c, consists of one segment with a uniform diameter and an antiumbrella structure. We also observed the junctions consisting of two segments of different diameters. An example of such junctions is shown in Figure 8d. The diameter of the larger segment is 228 nm, and that of the smaller one is 153 nm. The pore channels of both segments are aligned circularly around the long axis (Figure 8e). Between the two segments there is a slope, oriented along one of the three equivalent hexagonal lattice directions.

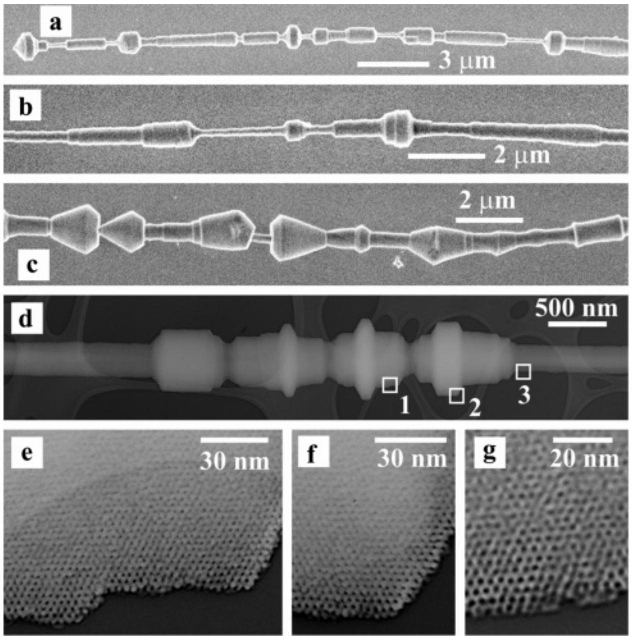

Figure 9. (a), (b), and (c) SEM images of artistic table-leg-like structures. (d) Low-magnification TEM image of one table-leg-like structure. (e), (f), and (g) are zoomed-in TEM images of the boxed areas labeled 1, 2, and 3 in (d). The samples were synthesized with C_{16}TMAB surfactant at 85 °C and prepared for SEM and TEM imaging without calcination.

Multiple segments of varying diameters and lengths can grow together along the fiber axis to form artistic table-leg-like shapes (Figure 9). These segments have diameters ranging from 150 nm to 1.5 μm and lengths ranging from 50 nm to 4 μm, and they are distributed within a total length of 10−60 μm. Their diameter-to-length ratios vary from 0.05 to 10. They have either cylindrical shapes (Figure 9, parts a, b, and d) or conical shapes (Figure 9c). TEM imaging at high magnifications reveals that the pore channels in all the segments are wound circularly around the common fiber axis (Figure 9, parts e, f, and g). The slopes at the junctions between two neighboring segments with different diameters are always oriented along one of the hexagonal lattice directions. The radius differences of adjacent segments can be as small as a few lattice constants and as large as 500 nm. The presence of such junctions suggests that the pore channels in these nanofibers are circular rings. If the pore channels were helices, the radius variation between adjacent segments would be smooth and the junctions would be irregular.

A three-dimensional model (Figure 10) can be built for the nanofibers with circular pore architectures on the basis of all the structural observations described above. Each nanofiber is composed of a large number of circular pore channels of various diameters packed hexagonally together. The hexagonal arrays of the pore channels observed at the edges of each nanofiber with the viewing direction perpendicular to the fiber axis during TEM imaging are cross sections through the fiber axis (Figure 6c). One interesting aspect about this type of nanofiber is that one translational symmetry is destroyed by curving the pore channels and a new

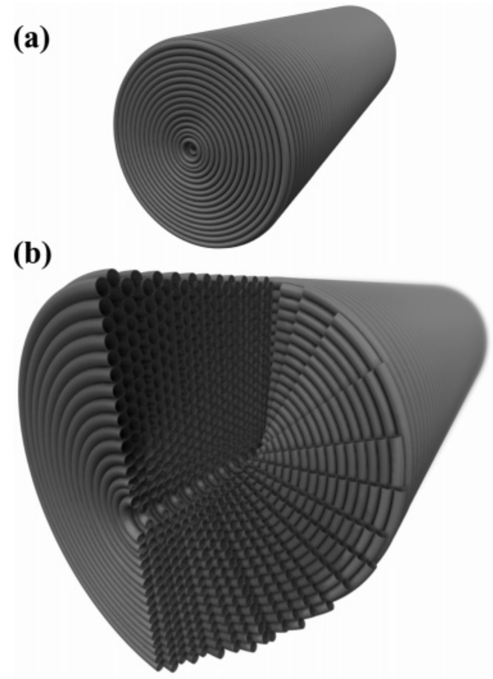

Figure 10. Three-dimensional model of a nanofiber with a circular pore architecture. (a) One complete nanofiber. (b) One portion of the nanofiber is cut away to reveal the internal organization of the pore channels.

rotational symmetry is established. The internal pore architecture of these nanofibers is significantly different from the two-dimensional hexagonal mesostructure. There have been few materials showing such rotational symmetry properties.

Temperature Dependence of Nanofiber Pore Architectures. It has been described above that mesoporous nanofibers can be synthesized using the one-phase route with C_{16}TMAC and C_{16}TMAB surfactants and that the internal pore architectures of the nanofibers can be selectively controlled by varying the growth temperature. We have found that C_{16}PC and C_{16}PB surfactants can also be used to prepare mesoporous nanofibers with the internal pore architectures controlled by the growth temperature. Figure 11a shows one example of the nanofibers synthesized with C_{16}PC surfactant at 45 °C. The nanofiber has a longitudinal pore architecture. Figure 11b shows one example of the nanofibers synthesized with C_{16}PB surfactant at 70 °C. Hexagonally packed pore channels are observed at the edges of each nanofiber, indicating that the nanofiber has a circular pore architecture.

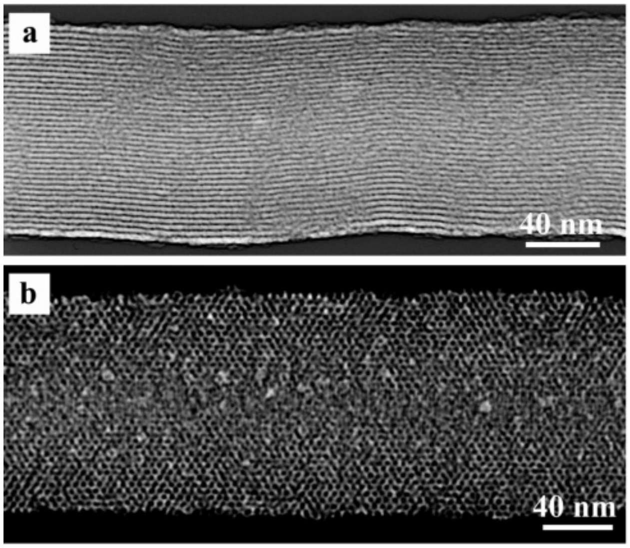

Figure 11. (a) TEM image of a nanofiber synthesized with C_{16}PC surfactant at 45 °C. The diameter of the nanofiber is 115 nm. (b) TEM image of a nanofiber synthesized with C_{16}PB surfactant at 70 °C. The diameter of the nanofiber is 127 nm. The samples were prepared for TEM observation without calcination.

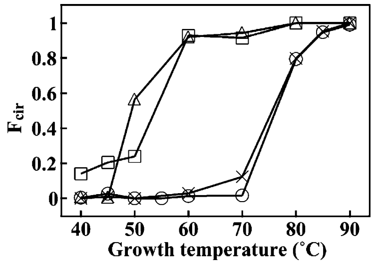

Figure 12. Fraction of the nanofibers with circular pore architectures (F_{cir}) as a function of the growth temperature. Circles, crosses, triangles, and squares represent that the nanofibers were synthesized with C_{16}TMAC, C_{16}TMAB, C_{16}PC, and C_{16}PB surfactants, respectively. The lines are guides to eye.

We carried out the syntheses of mesoporous nanofibers at various growth temperatures to investigate the dependence of nanofiber pore architectures on the growth temperature. Since the nanofibers that possess a number of kinks along the fiber axis always exhibit longitudinal pore architectures and the nanofibers that are relatively straight without kinks along the fiber axis always exhibit circular pore architectures, SEM imaging was used to quickly characterize the internal pore architectures of the nanofibers. Figure 12 shows the fraction of the nanofibers with circular pore architectures as a function of the growth temperature for C_{16}TMAC, C_{16}TMAB, C_{16}PC, and C_{16}PB surfactants. All the syntheses in Figure 12 were performed under similar conditions, except for the growth temperature. For each surfactant at each growth temperature, 300–500 nanofibers were counted. The yield of nanofibers from each synthesis generally decreases as the growth temperature is lowered. Only curve-shaped particles are obtained from the syntheses at temperatures below 40 °C.

As revealed in Figure 12, first, there is a general trend between the fraction of the nanofibers with circular pore architectures and the growth temperature for all the four surfactants. The syntheses at lower growth temperatures produce nanofibers with longitudinal pore architectures, and those at higher temperatures produce nanofibers with circular pore architectures. In the intermediate temperature regions, mixtures of nanofibers with either longitudinal or circular pore architectures are obtained. Second, the curve for C_{16}TMAC surfactant almost overlaps with that for C_{16}TMAB surfactant, and the curve for C_{16}PC surfactant almost overlaps with that for C_{16}PB surfactant. Lastly, the transition temperature from the nanofibers with longitudinal pore architectures to those with circular pore architectures is estimated to be 75 °C for hexadecyltrimethylammonium surfactants and 55 °C for hexadecylpyridinium surfactants, respectively.

Our nanofibers are synthesized under strongly acidic conditions, where the silica species in solutions are positively charged. Counterions are needed to mediate the interactions between cationic surfactant molecules and the positively charged silica species for the formation of mesoporous silica materials.[45−48] It has been known that the binding strengths of different anions to the micelles formed from cationic surfactants in aqueous solutions is different,[50] and the effects of various anions, including Cl^- and Br^-, on the morphologies and mesopore orientations of the mesoporous silica materials synthesized under acidic conditions have been demonstrated.[51] In our experiments, the trends between the fraction of the nanofibers with circular pore architectures and the growth temperature for C_{16}TMAC and C_{16}PC are observed to be almost identical to those for C_{16}TMAB and C_{16}PB, respectively, because the concentrations of HCl that were used are much larger than those of the surfactants in the growth solutions. For the syntheses with C_{16}TMAB and C_{16}PB, the molar ratio of Cl^- to Br^- in the growth solutions is ~350. Such a large difference in the amounts of Cl^- and Br^- in the growth solutions makes Cl^- ions dominate the mediation of the interactions between cationic surfactant molecules and the positively charged silica species during the growth of mesoporous nanofibers.

It has been shown previously that the synthesis temperature has a large effect on the surface area, pore size, pore volume, mesoscopic order, morphology, and type of mesostructures of resulting mesoporous materials.[52−56] In our experiments, we found that the internal pore architectures of mesoporous nanofibers can be controlled by varying the growth temperature. The dependence of the internal pore architecture on the growth temperature can be qualitatively understood by considering the Gibbs free energy of the formation of mesostructures. The free energy involved in the cooperative assembly of molecular silica species and surfactant molecules into the mesostructures of well-defined nanoscale organic and inorganic domains under acidic conditions has been proposed previously to be composed of four contributions, including (i) van der Waals and electrostatic interactions at the interface between organic surfactant and inorganic silica domains, (ii) interactions within the silica domains, (iii) van der Waals and conformational energies of surfactant hydrocarbon chains and van der Waals and electrostatic interactions of surfactant headgroups, and (iv) the chemical potential of the surrounding solution phase.[48] An additional contribution, (v) the solid−liquid interfacial energy between solid mesostructured products and the growth solution, should also be explicitly taken into account when the morphological sizes of the products are on the nanometer scale because the ratio of the external surface area to the volume of each nanoscale mesostructured entity is large. The free energy associated with the organization of amphiphilic surfactant molecules varies with temperature, as evidenced by the previous observations of the temperature dependence of the critical micelle concentrations of alkyltrimethylammonium and alkylpyridinium surfactants.[57] The temperature variation can also influence the electrostatic interactions between charged surfactant molecules and silica species and the chemical potential of the growth solution. As a result, the cooperative assembly between surfactant molecules and silica species produces the nucleation sites for mesostructured nanofibers with different internal pore architectures to minimize the overall free energy of the growth system. The minimization of the overall free energy is manifested by the fact that the nanofibers with circular pore architectures have round cross sections and that those with longitudinal pore architectures have hexagonal cross sections. The external surface area of the cylindrical fibers is about 95% of that of the hexagonal fibers at a constant cross-sectional area. The internal packing energy of mesostructured organic and inorganic domains in the hexagonal nanofibers with longitudinal pore architectures must somehow compensate for the increase in the external interfacial energy.

The transition temperature between the nanofibers with longitudinal pore architectures and those with circular pore architectures is ~75 °C for hexadecyltrimethylammonium surfactants and ~55 °C for hexadecylpyridinium surfactants, respectively. We believe that this difference in the transition temperature is due to the different headgroups possessed by the two types of surfactants. The sizes, shapes, and molecular configurations of surfactant headgroups play important roles in the aggregation of amphiphilic surfactant molecules to form micelles in aqueous solutions. The headgroup area of each hexadecyltrimethylammonium surfactant molecule at the micellar interface is 0.52 nm^2,[58] while that of each hexadecylpyridinium surfactant molecule is 0.58 nm^2.[59] The two types of surfactants have different critical micelle concentrations and enthalpies of micellization, and their critical micelle concentrations also exhibit different behaviors of temperature dependence. For example, the critical micelle concentrations of C_{16}TMAB and C_{16}PB at 40 °C are 0.95 and 0.45 mM, respectively. The enthalpies of micellization of C_{16}TMAB and C_{16}PB measured by microcalorimetry at 40 °C are −18.5 and −24.1 kJ/mol, respectively. The critical micelle concentration of C_{16}TMAB increases with rising temperature, but that of C_{16}PB decreases with rising temperature.[57,60,61] Further efforts are required to make quantitative measurements of the thermodynamic parameters involved in the growth of mesostructured

---

(50) Leontidis, E. *Curr. Opin. Colloid Interface Sci.* **2002**, *7*, 81.

(51) Lin, H.-P.; Kao, C.-P.; Mou, C.-Y.; Liu, S.-B. *J. Phys. Chem. B* **2000**, *104*, 7885.

(52) Matos, J. R.; Kruk, M.; Mercuri, L. P.; Jaroniec, M.; Zhao, L.; Kamiyama, T.; Terasaki, O.; Pinnavaia, T. J.; Liu, Y. *J. Am. Chem. Soc.* **2003**, *125*, 821.

(53) Kipkemboi, P.; Fogden, A.; Alfredsson, V.; Flodström, K. *Langmuir* **2001**, *17*, 5398.

(54) Galarneau, A.; Cambon, H.; Di Renzo, F.; Fajula, F. *Langmuir* **2001**, *17*, 8328.

(55) Wang, L.-Z.; Shi, J.-L.; Yu, J.; Zhang, W.-H.; Yan, D.-S. *Mater. Lett.* **2000**, *45*, 273.

(56) Prouzet, E.; Pinnavaia, T. J. *Angew. Chem., Int. Ed. Engl.* **1997**, *36*, 516.

(57) van Os, N. M.; Haak, J. R.; Rupert, L. A. M. *Physico-Chemical Properties of Selected Anionic, Cationic and Nonionic Surfactants*; Elsevier: New York, 1993; p 109−201.

(58) Okano, L. T.; Quina, F. H.; El Seoud, O. A. *Langmuir* **2000**, *16*, 3119.

(59) Bauer, A.; Woelki, S.; Kohler, H.-H. *J. Phys. Chem. B* **2004**, *108*, 2028.

(60) Barry, B. W.; Russell, G. F. J. *J. Colloid Interface Sci.* **1972**, *40*, 174.

(61) Vojtekova, M.; Kopecky, F.; Greksakova, O.; Oremusova, J. *Collect. Czech. Chem. Commun.* **1994**, *59*, 99.

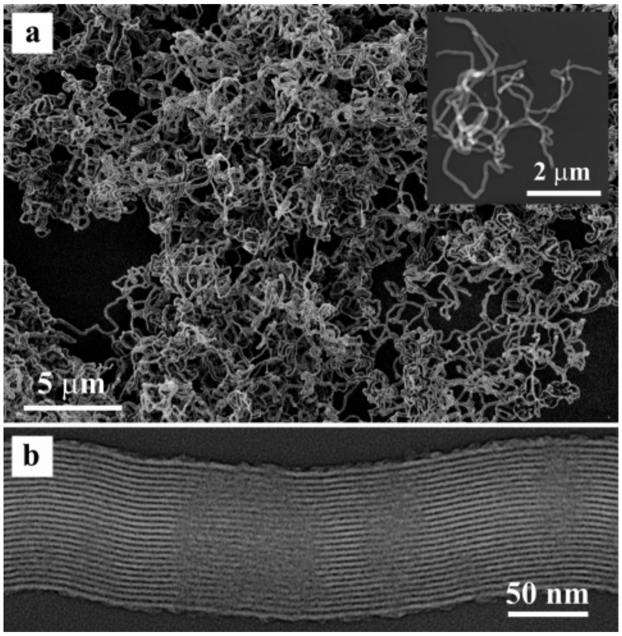

Figure 13. Nanofibers synthesized with C_{18}TMAB at 70 °C. (a) SEM image of the nanofibers. The inset is a low-magnification TEM image. (b) High-magnification TEM image of one nanofiber. The nanofibers were prepared for SEM and TEM imaging without calcination.

nanofibers to fully understand the temperature dependence of the internal pore architectures of the nanofibers.

Syntheses with C_{12}TMAB, C_{14}TMAB, and C_{18}TMAB. We further carried out the one-phase syntheses using alkyltrimethylammonium bromide surfactants of different hydrophobic tail lengths at various temperatures to obtain mesoporous nanofibers with different pore sizes. However, the synthesis with C_{12}-TMAB surfactant always produces spherical particles of diameters ranging from several hundred nanometers to several micrometers, and the synthesis with C_{14}-TMAB produces micrometer-sized curve-shaped particles (see Figure S2 in the Supporting Information). In contrast, almost all the products from the synthesis with C_{18}TMAB surfactant are mesostructured nanofibers. These nanofibers possess a large number of kinks along the fiber axis and are entangled together (Figure 13a), suggesting that they have longitudinal pore architectures. The longitudinal pore architecture is also corroborated by TEM images at high magnifications, in which the pore channels aligned parallel to the fiber axis are observed (Figure 13b). Moreover, the internal pore architectures of the nanofibers synthesized with C_{18}-TMAB surfactant are independent of the growth temperature in the range from 50 to 90 °C. They always have longitudinal pore architectures.

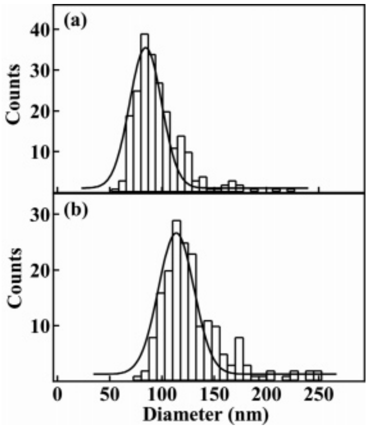

Figure 14. Diameter distributions of the nanofibers grown with C_{16}TMAC surfactant at growth temperatures of (a) 50 °C and (b) 85 °C. The solid lines are Gaussian fits to the diameter distributions. The total counted number of the nanofibers with longitudinal pore architectures is 222, and the bin size is 7.0 nm. For the nanofibers with circular pore architectures, the total counted number is 185 and the bin size is 7.5 nm.

We believe that the solid−liquid interfacial energy between the synthesis products and liquid growth solutions plays an important role here in the dependence of the morphological shapes of the synthesis products on surfactant tail lengths. The external surface areas increase in the order of spheres, curve-shaped particles, and nanofibers at a constant volume. Because the formation of mesostructured materials is determined by the interplay of the internal packing energy and the external interfacial energy, the increase in the external interfacial energy must be balanced by the decrease in the internal packing energy. In this sense, it is possible to control the morphological shapes of mesoporous materials by judiciously modifying the internal packing energy.

Diameter Distributions of Mesoporous Nanofibers. We have measured the diameter distributions of two batches of nanofibers that were grown in dilute C_{16}-TMAC surfactant solutions under similar conditions at different growth temperatures. One batch of nanofibers was grown at 50 °C, while the other was grown at 85 °C. About 50 TEM images were taken at low magnifications, and the diameters of ∼200 nanofibers were measured from digitized TEM images for each batch of nanofibers. Because nanofibers are twisted, it is difficult to measure the edge lengths of the hexagonal nanofibers with longitudinal pore architectures. These nanofibers are approximated to be cylindrical. Figure 14, parts a and b, shows the diameter distributions of the nanofibers with longitudinal pore architectures and those with circular pore architectures, respectively. The nanofibers with longitudinal pore architectures are generally smaller, with an average diameter of (84 ± 15) nm, while the nanofibers with circular pore architectures have an average diameter of (114 ± 17) nm. The diameter distributions for both types of nanofibers are not symmetric, with tails extending to ∼250 nm.

XRD, TGA, and Nitrogen Sorption Measurements. We have scaled up our synthesis to make bulk quantities of mesoporous nanofiber samples for low-angle XRD, TGA, and nitrogen sorption measurements. The low-angle XRD patterns of the nanofibers synthesized with C_{16}TMAC surfactant at 50 and 85 °C and those synthesized with C_{18}TMAB at 70 °C show up to four diffraction peaks (Figure 15), which can be indexed according to a two-dimensional hexagonal lattice. The lattice constants are determined to be 4.72, 4.73, and 5.27 nm for the nanofibers synthesized with C_{16}TMAC at 50 °C, at 85 °C, and those synthesized with C_{18}TMAB, respectively (see Table S1 in the Supporting Information for diffraction angles and corresponding *d* spacings). After calcination, all the diffraction peaks remain and

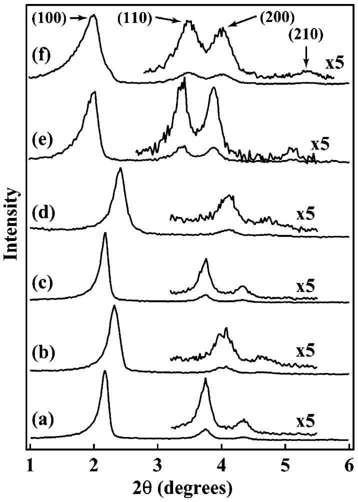

Figure 15. Low-angle XRD patterns of mesoporous nanofibers. (a) and (b) Nanofibers grown with C_{16}TMAC at 50 °C before and after calcination. (c) and (d) Nanofibers grown with C_{16}TMAC at 85 °C before and after calcination. (e) and (f) Nanofibers grown with C_{18}TMAB at 70 °C before and after calcination.

appear at higher diffraction angles. The lattice constants for the three nanofiber samples after calcination are determined to be 4.40, 4.31, and 5.14 nm, respectively. The low-angle XRD patterns taken on the curve-shaped particles that were grown together with the nanofiber samples synthesized with C_{16}TMAC at the two temperatures also show three diffraction peaks, and all three diffraction peaks remain after calcination (see Figure S3 in the Supporting Information). The determined lattice constants of the particles grown at 50 °C before and after calcination are 4.32 and 4.20 nm, respectively, and those of the particles grown at 85 °C before and after calcination are 4.59 and 4.39 nm, respectively (see Table S2 in the Supporting Information for diffraction angles and corresponding *d* values).

The retention of the three diffraction peaks after calcination indicates that the mesoscopic order is preserved in the calcined nanofiber samples. Since the XRD measurements show only the local hexagonal pore arrangement and cannot reveal if the overall fiber shape remains after calcination, TEM imaging was further performed on the calcined nanofiber samples with either longitudinal (Figure 16a) or circular pore architectures (Figure 16b). Both the overall fiber shape and the internal pore architecture are preserved after calcination. In addition, the parallel pore channels in the nanofibers with longitudinal pore architectures are open at the fiber end (Figure 16a, inset), which provides an opportunity for the incorporation of chemical species, for example, conjugated semiconducting polymers, into these nanofibers to make nanocomposite materials.[62]

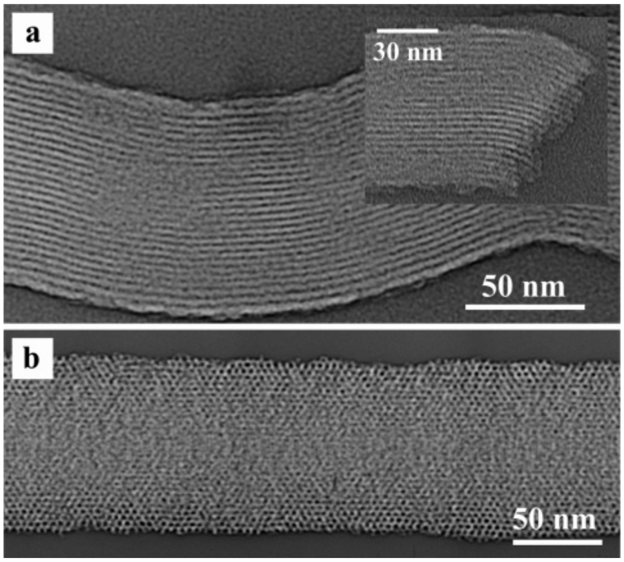

Figure 16. (a) TEM image of a calcined nanofiber synthesized with C_{16}PB surfactant. The fiber has a longitudinal pore architecture. The inset shows the parallel pore channels that are open at the fiber end. (b) TEM image of a calcined nanofiber synthesized with C_{16}TMAC surfactant. The fiber has a circular pore architecture.

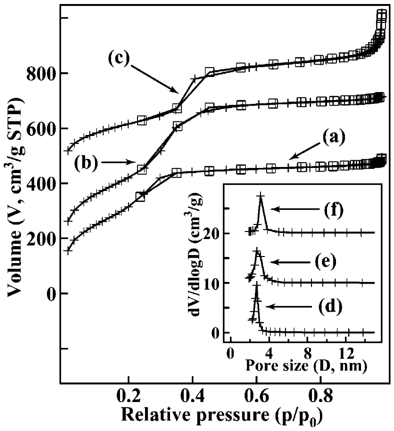

120

The

four

Figure 17. Nitrogen sorption isotherms of mesoporous nanofibers. (a) Nanofibers synthesized with C_{16}TMAC surfactant at 50 °C. (b) Nanofibers synthesized with C_{16}TMAC surfactant at 85 °C. (c) Nanofibers synthesized with C_{18}TMAB surfactant at 70 °C. Crosses represent the adsorption branches, and squares represent the desorption branches. The isotherms (b) and (c) have been shifted up 100 and 400 cm^3/g, respectively. (d), (e), and (f) in the inset show BJH pore-size distributions obtained from the adsorption branches of (a), (b), and (c), respectively. The pore-size distributions (e) and (f) have been shifted up 10 and 20 cm^3/g.

TGA and DTA traces recorded on the nanofiber and curve-shaped particle samples synthesized with C_{16}TMAC surfactant at 50 and 85 °C exhibit similar thermal behavior (see Figures S4 and S5 in the Supporting Information). The total weight losses for the four samples are all around 30 wt %. There are three distinct stages of weight loss for all the samples. The first one, up to 120 °C, is due to desorption of water. The second one, between 120 and 630 °C, is due to the combustion and decomposition of organic surfactants in air. The temperatures at which the sharp exothermic peaks are located are around 340 °C for all four samples. The initial fast and then slow loss of weight during the second step suggests that the thermal decomposition of the surfactants yields different products. The third step, from 630 °C to higher temperatures, is due to the water loss via condensation of silanol groups to form siloxane bonds.

The nitrogen sorption isotherms of calcined nanofiber samples are shown in Figure 17, and their pore characteristics are summarized in Table 1. The two types

---

[62] Nguyen, T. Q.; Wu, J. J.; Doan, V.; Schwartz, B. J.; Tolbert, S. H. *Science* **2000**, *288*, 652.

Table 1. Pore Characteristics of Mesoporous Nanofibers[a]

sample	S_{BET}[b] (m^2/g)	V[b] (cm^3/g)	d_{BJH}[b] (nm)	fwhm[b] (nm)
A	1200	0.75	2.7	0.5
B	1200	0.94	2.7	0.8
C	770	0.93	3.1	0.5

[a] A: nanofibers synthesized with C_{16}TMAC at 50 °C. B: nanofibers synthesized with C_{16}TMAC at 85 °C. C: nanofibers synthesized with C_{18}TMAB at 70 °C. [b] S_{BET}, BET surface area; V, single-point total desorption pore volume; d_{BJH}, BJH pore size; fwhm, the full width at half-maximum of the pore size distribution.

of nanofibers synthesized with C_{16}TMAC surfactant at 50 °C and 85 °C possess similar Brunauer−Emmett−Teller (BET) surface areas and pore volumes. The surface areas and pore volumes of the nanofibers are also similar to those measured on the curve-shaped particles that were grown together with the nanofibers (see Figure S6 and Table S3 in the Supporting Information). They all have a BJH pore size of 2.7 nm with narrow pore size distributions. In comparison, the nanofibers grown with C_{18}TMAB surfactant at 70 °C possess a BJH pore size of 3.1 nm, which is, as expected, larger than the pore size of the nanofibers made with hexadecyltrimethylammonium surfactants.

These measurements, including low-angle XRD, TGA, and nitrogen sorption, performed on bulk amounts of mesoporous nanofibers, on the one hand, indicate that the structure and pore characteristics of these nanofibers are similar to those of SBA-3 mesoporous materials synthesized under acidic conditions[45,46] because the pore channels in these materials are hexagonally packed. On the other hand, it is seen that these measurements cannot detect the structural difference between the nanofibers with longitudinal pore architectures and those with circular pore architectures. They cannot even differentiate between the nanofibers and the particles that were grown together. The inability to differentiate between the nanofibers and particles and between the two types of nanofibers using XRD, TGA, and nitrogen sorption highlights the importance of probing the internal pore architectures of individual mesoporous objects and correlating the pore orientations with the overall morphological shapes.

Growth Mechanism. In our experiments, we observed that the nanofibers with longitudinal pore architectures have uniform diameters along the fiber axis. For the nanofibers with circular pore architectures, a majority of them have uniform diameters along the fiber axis, and a significant amount of the fibers possess multiple segments of varying lengths and diameters. In addition, we also carried out the experiments to grow nanofibers by keeping growth solutions first at one temperature and then at another temperature. In one experiment, four batches of nanofibers were first grown with C_{16}TMAC surfactant at 50 °C for 3, 7, 14, and 24 h, respectively, and then they were kept at 85 °C for 2 days. In another experiment, four batches of nanofibers were first grown with C_{16}TMAC surfactant at 85 °C for 3, 7, 14, and 24 h, respectively, and then they were kept at 50 °C for 2 days. We have found that the nanofibers that were grown first at 50 and then at 85 °C always have longitudinal pore architectures and those that were first grown at 85 and then at 50 °C always have circular pore architectures (see Figure S7 in the Supporting Information). The internal pore architectures of the nanofibers are solely determined by the initial growth temperatures. On the basis of these observations, together with the fact that the lengths of the nanofibers are up to millimeters, we propose that the growth of the mesostructured silica nanofibers involves two stages. The first stage is the cooperative assembly between silica species and surfactant molecules to form nucleation sites. The second stage is the continuous growth of the nucleation sites into nanofibers. The internal pore architectures of the nanofibers are controlled in the first stage by the cooperative assembly process and its associated free energy changes.

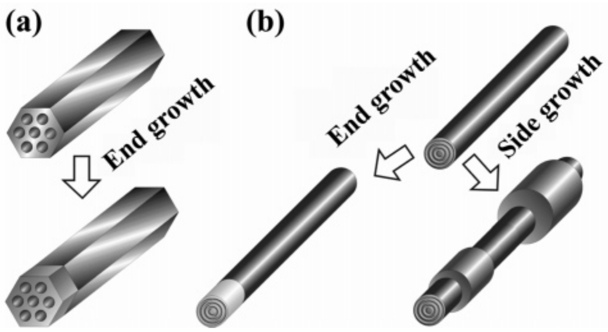

Figure 18. Proposed growth mechanism for mesoporous nanofibers. (a) End growth for the nanofibers with longitudinal pore architectures. (b) End growth and side growth for the nanofibers with circular pore architectures.

There are two continuous growth modes in the second stage (Figure 18). One is end growth, during which silica species and surfactant molecules coassemble to the ends of the nanofibers, and, thus, the nanofibers grow longer and longer. The other is side growth, during which silica species and surfactant molecules coassemble along the sides of the nanofibers, and, thus, the nanofibers grow thicker and thicker. We believe that only end growth is involved in the continuous growth of the nanofibers with longitudinal pore architectures because the diameter of each fiber is always uniform along the fiber axis. The growth of the nanofibers with circular pore architectures involves both end growth and side growth because a significant amount of the fibers exhibit junctions of varying lengths and diameters.

Fluorescent Nanofibers. Mesostructured nanofibers were doped with Rh6G dye molecules by adding a certain amount of Rh6G in the growth solution. The mesostructured silica is essentially composed of highly ordered inorganic and organic nanoscale domains. These domains can provide chemically different environments for various types of dyes. Depending on their hydrophilicity or hydrophobicity, these dyes can preferably be incorporated into inorganic or organic domains. Figure 19, parts a and b, shows the fluorescence images of the nanofibers synthesized at 85 °C and those synthesized at 50 °C, respectively. Each nanofiber fluoresces uniformly along the fiber axis. The fluorescence signal from the nanofibers synthesized at 85 °C is generally stronger than that from the nanofibers synthesized at 50 °C because the diameters of the former fibers are on average larger than those of the latter ones. The fluorescence spectra taken on the nanofibers doped with Rh6G molecules (Figure 19c) peak at 579 nm, which is in agreement with the previous results obtained on Rh6G-doped mesostructured fibers with micrometer-

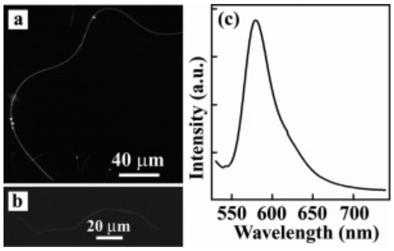

Figure 19. Fluorescent nanofibers doped with Rh6G dye molecules. (a) and (b) are fluorescence images of the nanofibers synthesized with C_{16}TMAC at 85 °C and those at 50 °C, respectively. The bright fluorescent spots are from the micrometer-sized curve-shaped particles that coexist with the nanofibers. (c) Fluorescence spectrum obtained on the nanofiber shown in (a).

scale diameters.[28] Lasing from individual fibers with micrometer-scale diameters has been demonstrated before because the light in the visible region can be efficiently confined inside those fibers.[27] In our case, the fibers have diameters around 100 nm. They might find applications in, for example, controlled drug delivery,[63] biosensing,[64] and sub-wavelength waveguiding.[65]

Conclusions

Highly organized mesoporous silica nanofibers have been synthesized under strongly acidic conditions with cationic alkyltrimethylammonium and alkylpyridinium surfactants. Detailed structure characterizations indicate that these nanofibers possess either a longitudinal pore architecture, in which the pore channels are aligned parallel to the fiber axis and are hexagonally packed, or a circular pore architecture, in which the pore channels are wound circularly around the fiber axis and the circular pore channels are also hexagonally packed. The cross sections of the nanofibers with longitudinal pore architectures are hexagonal, and those of the nanofibers with circular pore architectures are circular. The internal pore architectures of these mesoporous nanofibers can be selectively controlled by the growth temperature or surfactant type. These structure-selective syntheses add further understanding to the fundamental mechanism governing the cooperative assembly of organic and inorganic molecular species into three-dimensionally structured arrays. The insights thus gained can help in designing highly organized inorganic and organic hybrid functional materials, and even devices.[66,67] In addition, the nanofibers with the pore channels aligned parallel to the fiber axis could function as nanoscale conveyors for transporting and delivering chemical and biological species.[68,69]

Acknowledgment. This work is supported by Mitsubishi Chemical Center for Advanced Materials and by an IBM faculty award to Galen D. Stucky. This work made use of MRL Central Facilities supported by the MRSEC Program of the National Science Foundation under award No. DMR00-80034. We thank Beverly Y. Asoo for help with microtoming, Peter Allen for help with the artistic illustration of the internal pore architectures of mesoporous nanofibers, and Michael H. Bartl and John H. Harreld for helpful discussion.

Supporting Information Available: Characterization details, SEM images, low-angle XRD patterns, diffraction angles and corresponding *d* spacings, TGA and DTA traces, and nitrogen sorption isotherms of curve-shaped particles, TEM images of the nanofibers synthesized with C_{16}TMAC surfactant first at 50 °C for 14 h and then at 85 °C for 48 h and those synthesized first at 85 °C for 24 h and then at 50 °C for 48 h (PDF). This material is available free of charge via the Internet at http://pubs.acs.org.

CM049028Q

---

(63) Czuryszkiewicz, T.; Ahvenlammi, J.; Kortesuo, P.; Ahola, M.; Kleitz, F.; Jokinen, M.; Lindén, M.; Rosenholm, J. B. *J. Non-Cryst. Solids* **2002**, *306*, 1.

(64) Henke, L.; Piunno, P. A. E.; McClure, A. C.; Krull, U. J. *Anal. Chim. Acta* **1997**, *344*, 201.

(65) Tong, L. M.; Lou, J. Y.; Mazur, E. *Opt. Express* **2004**, *12*, 1025.

(66) Park, S.; Lim, J.-H.; Chung, S.-W.; Mirkin, C. A. *Science* **2004**, *303*, 348.

(67) Fan, H. Y.; Yang, K.; Boye, D. M.; Sigmon, T.; Malloy, K. J.; Xu, H. F.; López, G. P.; Brinker, C. J. *Science* **2004**, *304*, 567.

(68) Regan, B. C.; Aloni, S.; Ritchie, R. O.; Dahmen, U.; Zettl, A. *Nature* **2004**, *428*, 924.

(69) Rustom, A.; Saffrich, R.; Markovic, I.; Walther, P.; Gerdes, H.-H. *Science* **2004**, *303*, 1007.